Journal of Materials Chemistry C

Accepted Manuscript

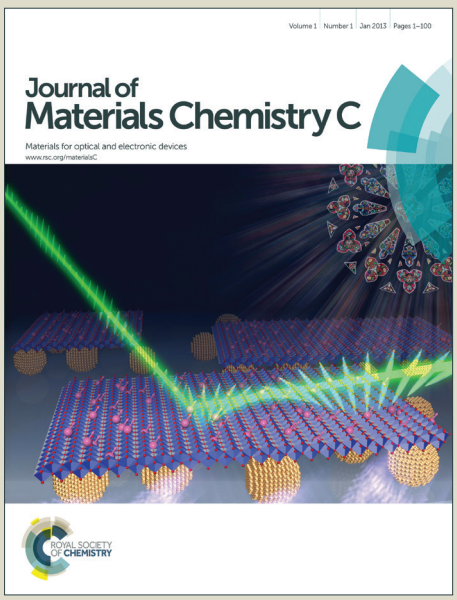

ROYAL SOCIETY OF CHEMISTRY

www.rsc.org/materialsC

Journal Name

RSCPublishing

ARTICLE

A bottom-up fabrication method for the production of visible light active photonic crystals

Cite this: DOI: 10.1039/x0xx00000x

Sibu C. Padmanabhan,[*a,b] Keith Linehan,[a] Shane O'Brien,[a] Syara Kassim,[a,c] Hugh Doyle,[a] Ian M. Povey,[a] Michael Schmidt,[a] and Martyn E. Pemble[*a,b]

Received 00th January 2012,
Accepted 00th January 2012

DOI: 10.1039/x0xx00000x

www.rsc.org/

A method which combines polymer particle assembly, chemical infiltration and etching with an aerosol assisted deposition process is described for the fabrication of 3D inverse opal (IO) structures with sub-micron periodicity and precision. This procedure not only overcomes limitations associated with slow, expensive micro-fabrication methods but also permits the tuning of refractive index contrast via the direct incorporation of photonically-active, preformed, tailored silicon nanostructures. It is demonstrated that this approach can be used to modify the photonic band gap (PBG) by effectively depositing/patterning optically active silicon nanocrystals (ncSi) onto the pore walls of a 3D inverse opal structure. This simple, yet effective method for preparing functional complex 3D structures has the potential to be used generically to fabricate a variety of functional porous 3D structures that could find application not only in new or improved photonic crystal (PC) devices but also in areas such as catalysis, separation, fuel cells technology, microelectronics and optoelectronics.

Introduction

Colloidal PCs, often also referred to as synthetic opals due to their resemblance to natural opal gemstones in certain cases, are periodic dielectric structures that possess photonic stop-bands which arise by virtue of their dielectric periodicity.[1-7] Depending on the frequency range where the stop-band is formed, photonic crystals can control the propagation of relevant photons. While the propagation of photons of frequency within the stop-band is forbidden, all other photons are allowed to propagate.[8-13] In an ideal case, the lattice spacing, and the dielectric contrast of the composite determine the photonic stop-band properties.[14-16] Tuning of these parameters has been shown to improve the stop-band properties to the extent to which the stop-band formed is able to restrict photon propagation within the whole of the optical Brillouin zone, i.e. irrespective of the propagation direction. Such a stop-band is also known as full PBG in contrast to the more directional pseudo gaps which are often observed for lower refractive index contrast media.[17-20] Although periodic structures with full PBGs have been realized at the longer wavelength region (above near-infrared) of the electromagnetic spectrum using 3D PC structures,[21-25] the realization of full PBGs at the visible light frequencies still remains a challenge. The major bottlenecks hindering its successful realization are (i), the inherent limitation and high costs associated with the use of top-down micro-fabrication approaches in creating 3D structures with precise sub-micron periodicity and (ii), the unavailability of suitable high dielectric materials having negligible absorption in the visible frequency range.

The generic aim of most photonic crystals research is to achieve control over the manipulation and utilization of photons in order to enable novel technological platforms.[26-34] While control over spontaneous emission is at the heart of many potential photonic crystal-based technologies,[3,25,35-37] more and more exciting avenues are driving the research into new application areas.[27,38-40] For example the use of photonic crystals in solar cells and sensors, and also the effective utilization of diffuse scattering by photonic crystals to enhance LED lighting efficiency. This latter application is one example of this technology where the formation of a complete PBG is not a specific requirement.[33,41]

Of direct relevance to this type of application we show here how the two-in-one functional properties of pre-formed silicon nanocrystals-namely their high refractive index and tuneable photoluminescence (PL) emission, can be effectively utilized to improve first the visible light PBG properties as evidenced by the broadening of the stop-band and the overlap of specific features in the reflectance spectra and then to demonstrate the modification of PL emission in the presence of the altered PBG. The method presented here is straightforward and potentially scalable to large area fabrication of robust 3D inverse opal structures. Importantly, the method described[42,43] does not require the use of any complicated deposition, annealing[43] and etching processes.

Experimental

Synthesis of PMMA colloidal particles

Methyl methacrylate (MMA) and potassium persulfate were purchased from Aldrich. Millipore water (18.2 MΩ.cm) was used as the medium of reaction. The PMMA colloid of mean particle size 290 nm (relative standard deviation <5 %) was prepared by an emulsifier-free emulsion polymerization in water in the presence of the initiator potassium persulfate at a reaction temperature of 80° C. The reaction mixture was kept stirring throughout the reaction at a speed of 500 RPM. De-ionized water was first bubbled with nitrogen gas for 20 minutes. After this, 15 mL of MMA was added under nitrogen atmosphere followed by 0.19 g of potassium persulfate. The solution was then heated to 80^{o} C and maintained at this temperature for 40 minutes for the completion of the polymerization. After the polymerization reaction, the colloid was centrifuged and washed 5-6 times using Millipore water and used.

Preparation of silica inverse opal (SIO) templates

The SIO templates were prepared by a controlled evaporation self-assembly method, slightly modified from the previous reports[44,45] in order to combat the PMMA swelling issue, from a colloidal dispersion containing PMMA particles and pre-hydrolyzed tetraethyl orthosilicate (TEOS), onto a clean glass substrate placed in a slanted position in a glass vial. Precisely, 0.1 V % (8 mL) of PMMA particles of mean particle size 290 nm was allowed to evaporate at a temperature of 65° C in presence of 0.16 ml of pre-hydrolyzed TEOS precursor solution prepared by mixing acetic acid, TEOS and Millipore water in the volume ratio (1:1:8). Acetic acid here plays a dual role as chelating agent and acid catalyst for the polymeric hydrolysis of the TEOS precursor to produce a homogeneous silica sol.[46,47] The use of acetic acid also helps to avoid the use of ethanol which induces swelling of the PMMA particles. The formed opal is then immersed in acetone for 2h with changing the solution a couple of times for a complete dissolution of the PMMA template to obtain the inverse opals.

The opal templates were then characterized using a Perkin-Elmer Lambda 950 spectrophotometer for their PBG properties. Angle-resolved reflection spectra of the samples were acquired at varying angles of incidence, θ, with respect to the (111) surface normal from 8° to 65° for the wavelength range of 200 – 2000 nm. For that, the samples were illuminated by a collimated beam of UV/Vis/NIR light with a spot diameter of 5 mm x 5 mm obtained from pre-aligned tungsten-halogen and deuterium sources. A combination of high performance Peltier-cooled InGaAs and PbS detectors were used for signal detection.

Chemical synthesis and purification of silicon nanocrystals

The synthesis of the Si nanocrystals is adapted from the method reported by Tilley and co-workers.[48] All reagents and solvents were purchased from Sigma-Aldrich Ltd. and used as received. In nitrogen filled glove-box, 0.00274 mol of tetraoctylammonium bromide (TOAB) was dissolved in 100 mL anhydrous toluene. 1.0 mL (0.0087 mol) $SiCl_4$ was added to the above solution and the mixture was left to stir for 30 min. Si nanocrystals were then formed by the drop wise addition of 6 mL of 1 M lithium aluminium hydride in THF over a period of 2 min. The solution was then left to react for 2.5 h. The excess reducing agent was then quenched with the addition of 60 mL methanol, upon which the dispersion became transparent. At this stage of the reaction, the silicon nanocrystals are terminated by hydrogen and encapsulated in a TOAB micelle. Chemically passivated nanocrystals were then formed by modifying the silicon-hydrogen bonds at the surface through addition of 200 μL of a 0.1 M H_2PtCl_6 in isopropyl alcohol as a catalyst followed by 6 mL of allylamine. After stirring for 2.5 h, the Si nanocrystals were removed from the glove box and the organic solvent was removed by rotary evaporation. The resulting dry powder (consisting mainly of surfactant) was then redispersed in 50 mL of distilled water and sonicated for 30 min. To remove the surfactant , the solution was first filtered twice using PVDF membrane filters (MILLEX-HV, Millipore 0.22 μM), after which the doubly filtered solution was concentrated down to 1 mL and purified via column chromatography using Sephadex gel LH-20 as the stationary phase. Fractions were collected every 50 drops at a flow rate of a drop every 5 s. A hand held UV lamp (365 nm) was used to check each fraction for Si nanocrystal luminescence. The fractions were then combined and reduced to a total volume of 20 mL.

Characterisation of silicon nanocrystals

PL spectra with an excitation wavelength of 325 nm were recorded on a Perkin Elmer LS 50 luminescence spectrophotometer equipped with a pulsed Xenon discharge lamp and Monk-Gillieson monochromators. PL spectra of the silicon nanocrystal dispersions were recorded at room temperature using a quartz cuvette (1 cm), while spectra of the SIO and ncSi-SIO samples were recorded using a custom-built front face illumination insert. For that the opal sample was held at an angle of 22.5 degrees with respect to the excitation beam. The excitation and detection pathways were kept at standard 90 degree angle. Transmission Electron Microscopy (TEM) images were recorded using a JEOL 2100 electron microscope operating at 200 KV and equipped with a LAB_6 electron source. TEM samples were prepared by depositing evaporating aliquots of the silicon nanocrystal dispersion onto a carbon coated TEM grid.

Aerosol-assisted infiltration of silicon nanocrystals

A modified aerosol-assisted chemical vapour deposition (AACVD)[49] system consisting of a tubular quartz reactor containing a graphite susceptor was used for nanocrystal infiltration. 10 mL of nanocrystal solution (ncSis in water with a concentration of ca. 30 x 10-6 ML^{-1} (30 micromolar) was held in a container above the metal diaphragm of a modified commercially available ultrasonic humidifier to form an

aerosol. The aerosol generated was swept into the reaction zone using a nitrogen carrier gas (1.58 L/min) metered from a mass flow controller. The sample was maintained at 200^{o} C during exposure to the aerosol. The exposure time of the opal sample to the aerosol was 45 minutes. This sample was named as ncSi-SIO-1 and the sample prepared with double its concentration (60 μ*M*) ncSi as ncSi-SIO-2 in the following discussions.

Electron microscopy analysis of the opals

The top-view and cross-sectional scanning electron microscope (SEM) images of the IOs before and after ncSi deposition are obtained using a FEI Quanta 650 FEG High Resolution SEM. TEM cross section sample was prepared using Focused Ion Beam (FIB) (FEI DualBeam FIB Helios Nanolab 600i). At first, the top of the opal sample was deposited/protected with layers of carbon and platinum by electron beam induced deposition (EBID) method. After depositing a thicker ion beam induced (IBID) protection layer of platinum the lamellae is cut out and attached to a TEM grid. Then the lamellae are thinned down to approx. 300-500 nm using the FIB at 30kV. The final polishing is done with 2kV in order to minimize the FIB induced damage to 2 nm per side. The targeted final thickness is in the range of 200-400 nm to represent one opal layer thick sample. The cross sections are analyzed at 200kV with JEOL JEM-2100 TEM with Oxford Inca EDX.

Results and Discussion

In order to probe the structural periodicity as well as the extent and consistency of the opal structures; and to compare the micro structural change occurred for the IO before and after silicon nanocrystal incorporation, SEM top-view and cross-sectional images were obtained. The SEM images are taken from the same opal sample before and after silicon nanocrystal incorporation for an unambiguous comparison. **Fig. 1** shows SEM top-view and cross-section images of the SIOs before (**Fig. 1a and 1b**) and after nanocrystal incorporation (**Fig. 1c and 1d**). As the SEM of the opal before nanocrystal incorporation was recorded without the use of gold/palladium sputtering designed to reduce charging effects, the image quality is a little compromised as a result of charging effects. However, the SEM images show the extensive 3D connectivity in the SIO structure. The high quality of the inverse opal template can be appreciated from the fact that the three-coordinate interconnects from the second, third and the subsequent layers underneath can be observed. The incorporation of ncSis can be appreciated from the difference in surface texture of the silica skeleton (walls) supporting the air spheres. While the SIO shows smooth silica walls, nanocrystal incorporation made the walls thicker and rougher. A corresponding reduction in the air sphere diameter is also observed, where the air sphere diameter reduced from 295 nm for the SIO to 281 nm for the ncSi-SIO-2. The presence of nanocrystals in the structure is further confirmed by TEM analysis from a cross-section obtained by FIB slicing. The TEM cross-section image presented in **Fig. 1e**, the selected area electron diffraction (SAED) pattern obtained from the area highlighted by a rectangular box in **Fig. 1e** (**Fig. 1f**) and the SAED pattern of the pre-formed silicon nanocrystals (**Fig. 1h)** all confirm the nature and presence of the nanocrystals in the structure. The SAED patterns show the presence of {331} and {113} planes of silicon. The diffuse nature of the ring patterns indicates that the nanocrystal surfaces may be partially oxidized, which is not surprising. The TEM image of the pre-formed nanocrystals is presented in **Fig. 1g**. The particle size distribution tabulated from the TEM image (inset of **Fig. 1g**) shows that ncSi particles are formed in the size range 2.5 – 5 nm by the described method.

The robustness of the structure can be appreciated from the fact that the 12 layer thick composite SIO structure remained intact against collapsing even after FIB slicing to just a thin cross-section (**Fig. 1e)**. This thin slice could withstand the pressure applied from the protective carbon/platinum plating employed prior to the FIB milling. We believe that the deformation of the top four layers of the template from spherical 'holes' towards a more egg-like shape is due to the pressure induced on from the platinum/carbon plating. The presence of platinum can be observed as a black infiltrate at the top layer (on the right hand side) of the composite SIO. Furthermore, the ability of the method to prepare robust large area, large domain size composite SIOs and SIO opals can be appreciated from the large area SEM images presented in the electronic supplementary information 1 (ESI 1).

The stop-gap properties of the samples were evaluated by recording the reflection spectra of samples at varying incidence angles, θ, 8° to 65° to the surface normal using a Perkin-Elmer Lambda 950 spectrophotometer in the wavelength range 200 – 2000 nm. The reflection spectra were recorded from the same SIO sample from almost the same spot before and after silicon nanocrystal incorporation. Figure 2a shows the optical reflection spectra of SIO, modified ncSi-SIO-1 (deposited from 10 mL of silicon nanocrystal solution of concentration ca. 30 x 10-6 ML^{-1} and modified ncSi-SIO-2 (deposited from a 10 mL silicon nanocrystal solution having twice the amount of silicon nanocrystals) samples recorded at 8° incidence. **Figs. 2b, 2c** and **2d** show the optical reflection spectra of SIO, ncSi-SIO-1 and ncSi-SIO-2 samples recorded at incidence angles 8° to 30° to the opal surface normal.

As may be seen the incorporation of silicon nanocrystals resulted in a 44 nm red-shift of the stop-band for ncSi-SIO-2 (λ_{max}, 672 nm) and a 32 nm red-shift for the stop band of ncSi-SIO-1 (λ_{max}, 660 nm) as compared to the bare SIO (λ_{max}, 628 nm). In addition to the red-shift, both the first order and second order stop-bands of ncSi-SIO-2 (672 nm and 371 nm respectively) show significant band broadening compared to the bare SIO (628 nm and 324 nm respectively). In contrast the reduced level of silicon nanocrystal incorporation via growth from the more dilute solution (ncSi-SIO-1) resulted in only a moderate band broadening for the ncSi-SIO-1 sample. As a

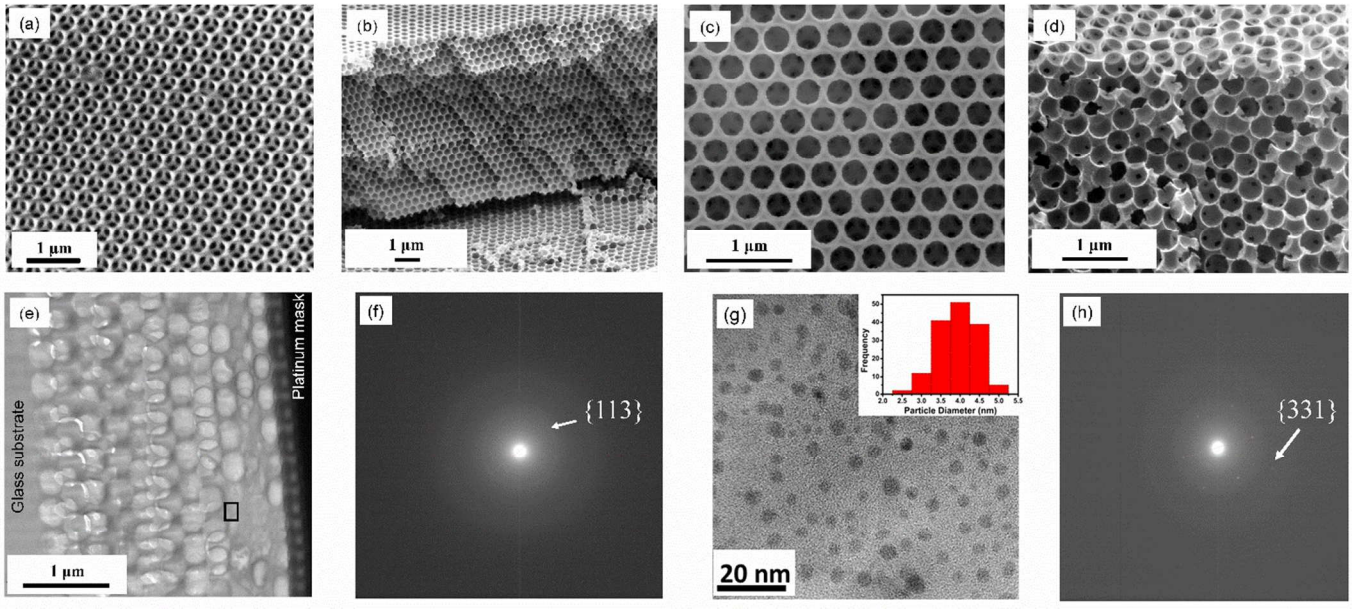

Fig. 1. SEM top view image of SIO (a), and cross-section image of the same opal template (b). SEM top view image of opal infiltrated with silicon nanocrystals (ncSi-SIO-2) (c), and cross-section image of the same sample (d). (e) TEM cross-section image of ncSi-SIO-2 prepared by FIB milling. (f) SAED pattern from the area highlighted by a black rectangular box in image (e). (g) HRTEM image of ncSis used for deposition with its histogram representing particle size distribution in the inset. (h) SAED pattern of preformed ncSi shown in image (g). The rings represent the {113} and {331} planes of silicon.

PBG, has increased from ~6.6% for SIO to ~7.3% for ncSi-SIO-1 and to ~18.0% for ncSi-SIO-2 samples in the incidence angle range 8° to 30°. The band broadening in turn resulted in an enhanced spectral overlapping for the ncSi-SIO-2 (**Fig. 2d)**, for incidence angles 8° to 30°, as compared to the more dispersive stop-bands for the bare SIO (**Fig. 2b**) and ncSi-SIO-1 samples.

This result demonstrates the efficacy and tunability of the aerosol-assisted infiltration method for the incorporation of silicon nanocrystals into the SIO template. The effect of nanocrystal incorporation can also be evidenced from the modification of the effective refractive indices (n_{eff}) for the ncSi-SIO-1 and ncSi-SIO-2 samples as compared to the bare SIO, as calculated from the plot of $\sin^2\theta$ *vs* λ^2_{max} (**Fig. 2e**). The n_{eff} is increased to 1.22 for ncSi-SIO-1 and further to 1.40 for ncSi-SIO-2 from that of 1.12 for the bare SIO. The refractive indices of the composite silicon nanocrystal/silica backbone have increased to 1.69 and 2.16 for ncSi-SIO-1 and ncSi-SIO-2 samples respectively from that of 1.40 for bare silica backbone of SIO. All of these data were obtained from the optical data by solving the Bragg-Snell relation for photonic crystals: $\lambda^2_{max} = 4d^2\left(n^2_{eff} - sin^2\theta\right)$; where λ_{max} is the wavelength maximum of the reflectance band, d is the lattice spacing, n_{eff} is the effective refractive index of the photonic crystal, and θ is the angle of incidence of the impinging electromagnetic radiation to the photonic crystal surface normal.[50,51]

Furthermore, above 30° incidence, the simultaneous multiple Bragg diffraction-induced multiple Bragg-wave coupling from the (111) and (200) planes of the inverse opal resulted in the modification of the stop-bands[52] (not shown here). As a result the $\Delta\lambda/\lambda$ further increased to >12% and >30% for ncSi-SIO-1 and ncSi-SIO-2 respectively from that of ~8% for SIO. In addition, a less intense, almost non-dispersive band is observed at the high frequency region (~230 nm) for the modified SIO samples (**Fig. 2a**). This feature is assigned to be due to the Van Hove singularities indicating the presence of good periodicity in the 3D IO structure.[53-55]

Despite resulting in band broadening and some spectral overlap, silicon nanocrystal incorporation has resulted in enhanced stop-bands for the nanocrystal composite ncSi-SIO samples as compared to the bare SIO, as evidenced from the increase in the gap to mid-gap ratio. However the reflectance properties of ncSi-SIO sample is reduced over an order of magnitude due to the loss mechanisms as discussed in the following discussion.

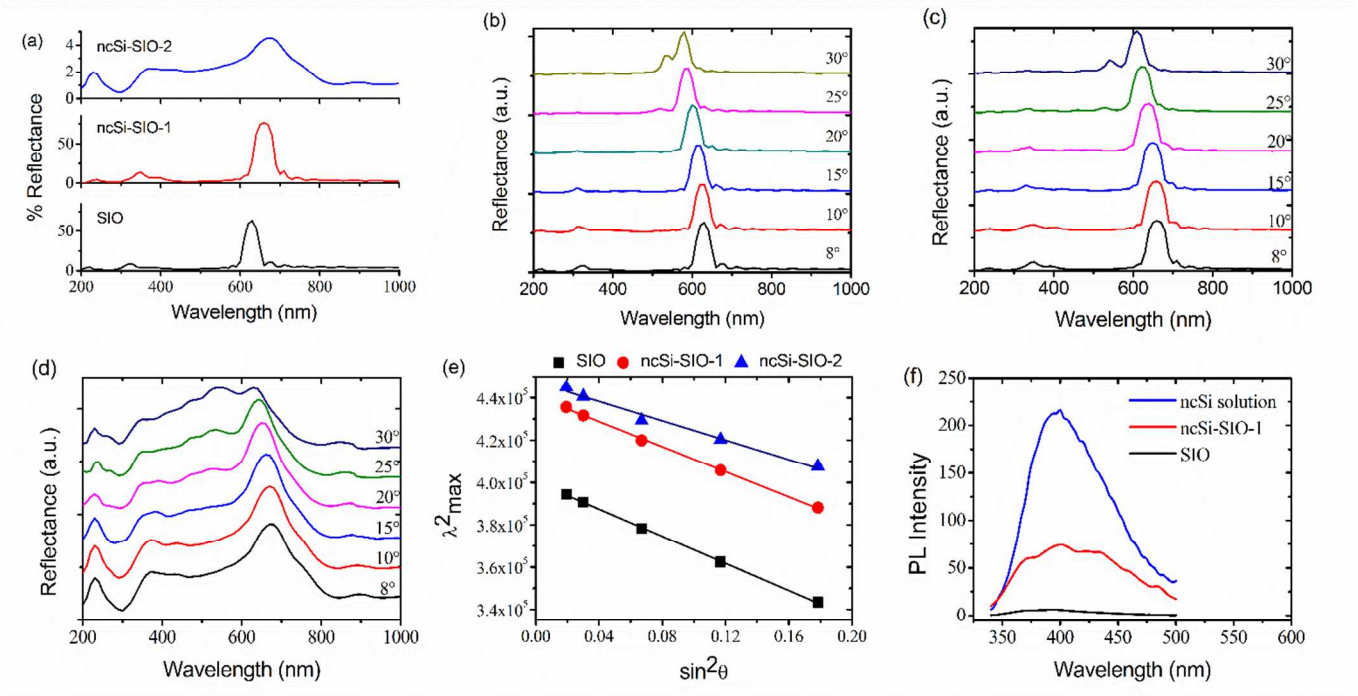

Fig. 2. (a) Reflection spectra of SIO, ncSi-SIO-1 and ncSi-SIO-2 samples recorded at an incidence angle of 8° to the opal surface normal. (b) Angle-resolved reflection spectra of SIO (c) ncSi-SIO-1 and (d) ncSi-SIO-2 samples recorded at incidence angles 8° to 30°. (e) Plot of $\sin^2\theta$ *vs* λ^2_{max} of the three opals. (f) PL emission spectra of ncSi-SIO-1, SIO (both collected at 60° angle to the opal surface normal) and ncSi solution.

The increase in refractive index contrast is modest- and not as large as that which has been achieved previously in all silicon inverse opals prepared by other methods.[56] However, the significant red-shift (44 nm) in the stop-band as well as its reduced dispersion, which reflects its tendency to form a complete PBG, as compared to the SIO sample, indicates the clear influence of the formation of a thin layer of silicon nanocrystals on the SIO walls for the composite SIO samples. Although the near non-dispersive nature of the stop-bands of composite SIO samples theoretically suggests that nanocrystal infiltration is isotropic and occurs on all exposed walls of the SIO structure, it is possible that the diminished stop-bands arise from enhanced scattering effects and/or possible interference from the organics used for ncSi synthesis and functionalization[57]- in other words such effects may arise because the nanocrystalline silicon may contain lower refractive index contamination.

The realization of ncSi patterning onto the walls of SIO structure was further examined by PL emission studies. In principle, the light emitted from the semiconductor ncSis should be modified in presence of the dielectric periodicity of the ncSi-SIO structure. [29,30,58-65] **Fig. 2f** shows the PL spectra of ncSi prior to deposition (blue line), SIO (black line) and ncSi-SIO-1 (red line). Since in the PL measurements, the emitted light is collected at 60° angle with respect to the opal surface normal, the reflection and transmission spectra of ncSi-SIO-1 sample measured at 60° incidence is also recorded and presented in ESI 2. The ncSi solution used here is characterized with a broad emission centred at ~400 nm,[66] possibly resulting from factors such as (i), the excitonic emission of nanocrystals of diameter <5 nm[67-70] (ii), the modification of said emission by the amine surface passivation employed and (iii), possible charge carrier recombination at the oxidised surfaces.[71,72] The modified emission of ncSis when integrated into the SIO-1 structure shows almost similar spectral features but with a comparatively lower intensity. The SIO sample prior to deposition on the other hand exhibits a negligible background emission. The fact that the PL emission does not fall in the band-edge wavelength of the ncSi-SIO opal theoretically rules out the enhancement of PL emission. The slightly attenuated/diminished PL emission in this case may be attributed to the effect of the diffuse scattering resulting from the presence of disorder (dislocations, point defects and line defects) inherent to the SIO structure, to possible absorption losses due to the ncSis, as well as to a possible interference from the roughened interfaces of the ncSi-SIO structure, which happens to be higher at the higher energy region of the stop-band.[73] Overall, the observation of much of the ncSi PL emission spectrum despite the presence of various loss mechanisms underlines the efficacy of 3D patterning by the method presented here.

The method described here is significant considering its ability to integrate functional materials into complex 3D structures by a simple process. Furthermore the preparation of integrated-

silicon inverse opals as described here may have potential technological implications in view of the ability of silicon to be integrated with many existing industrial processes. For example as noted earlier silicon has already been identified as one ideal material for the development of complete PBGs in 3D photonic crystals[22,54,55,74,75] although germanium has also been used due to its similarities in properties to silicon.[20,76-79]

Concerning the specific topic of optimising the PBG properties in silicon based photonic crystals previous reports have focused on the fabrication of silicon inverse opals by means of colloidal crystal templating,[80] i.e. by first depositing crystalline silicon into a silica photonic crystal template using chemical vapour deposition of a suitable precursor[75] followed by removal of the silica template by chemical dissolution.[54] However, the complexity of the method, involving as it does many intricate fabrication steps, and in particular the harsh HF chemical dissolution step, may pose serious limitations when it comes to maintaining the robustness of the structure and the reproducibility and scale up of the process.

To the best of our knowledge, all previous silicon based methods have demonstrated mostly near-infrared to infrared PBG properties. The effective integration of silicon into the photonic crystal template without compromising its structural periodicity and robustness has been a challenge for the development of visible light responsive photonic crystals. The method presented here is simple, straightforward and clearly addresses many of the limitations of the previously reported methods. Firstly, the large area, robust SIOs can be prepared by a mild chemical leaching method, just by immersing the PC in acetone, which avoids the harsh HF etching processes as has been used by the previously reported methods. The use of this sacrificial PMMA template is hence very significant in this method, because of its complete leachability in acetone. Secondly, the use of SIO as template allows an effective and straightforward deposition of ncSi due to its highly accessible interconnected larger spherical air spaces than just the narrow and small void spaces in 3DPCs. The successful realization of the 3D patterning of ncSi here is achieved by combining these two straightforward processes, hence making it simple yet scalable.

In addition previous methods adopted for the preparation of sub-micrometric 3D inverse opals were based on the deposition of the required dielectric/functional material into the voids of self-assembled opal templates by means of chemical infiltration followed by reduction,[78,81,82] electrodeposition,[38,83-86] atomic layer deposition (ALD)[87-90] or by CVD.[22,39,54,91] Although these methods have enabled the experimental validation of some of the unique optical properties of high dielectric contrast PCs, the extensive use of them may be limited due to a number of factors such as the complexity of the steps involved, the structural fragility of the opals prepared, as well as their limitations in achieving a uniform infiltration/deposition. Although ALD enables an atomic level conformal deposition of functional materials into the template void spaces,[92] the lengthy cycles (time and cost) needed is a matter of concern in many application fields.

Conclusions

In conclusion, we have presented a simplified fabrication of 'tuneable'[93] silicon-silica inverse opals using a colloidal crystal templating method combined with aerosol-assisted nanocrystal infiltration within the inverse opal. This method enables the 3D patterning of ncSis into robust silicon-silica inverse opals of larger areas and domain sizes. The highly accessible and robust 3D air spheres facilitated an effective deposition of ncSis onto all the available 3D silica walls in the structure. The method offers a significant advancement on the effective integration of functional/high dielectric materials into complex 3D structures. While the effective integration of ncSis facilitates photonic stop-band broadening and subsequent spectral overlap in the visible light frequency region, the flexibility of tuning the ncSi PL emission by a pre-deposition step should enable an effective control of light emitting features with respect to the PBG, thus offering great promise for future photonic technologies. Currently we are in the process of tuning the template photonic stop-gap frequencies and ncSi PL emission for the enhancement of the efficiencies of LED devices. Finally we note that the method of introducing the ncSi is quite generic and could also be used to incorporate other nanostructured materials including plasmonically active metal particles, biologically active nanoparticles or particles having tailored catalytic activity.

Acknowledgements

The work was supported by the Science Foundation Ireland (SFI PI 07/IN.1/1787). We thank EMAF, Tyndall for providing the microscopy facilities. We also thank the University of Malaysia Terengganu for a PhD studentship for Ms Kassim

Notes and references

[*]Authors for correspondence, Email: martyn.pemble@tyndall.ie; Fax: +353214904467; Tel: +353214906456.

[a]Tyndall National Institute, University College Cork, Lee Maltings, Cork, Ireland

[b]Department of Chemistry, University College Cork, College Road, Cork, Ireland,

[c]Universiti Malaysia Terengganu, Kuala Terengganu, Terengganu, Malaysia

Electronic Supplementary Information (ESI) available: SEM images of ncSi-SIO-1, large area SEM image of SIO, reflection/transmission spectra of ncSi-SIO-1 at 60° incidence and the UV-Vis absorbance spectrum of ncSi solution. See DOI: 10.1039/b000000x/

References

(1) Bogomolov, V. N.; Gaponenko, S. V.; Germanenko, I. N.; Kapitonov, A. M.; Petrov, E. P.; Gaponenko, N. V.; Prokofiev, A. V.; Ponyavina, A. N.; Silvanovich, N. I.; Samoilovich, S. M. *Physical Review E* **1997**, *55*, 7619.
(2) John, S. *Phys. Rev. Lett.* **1987**, *58*, 2486.
(3) Yablonovitch, E. *Phys. Rev. Lett.* **1987**, *58*, 2059.
(4) Kosaka, H.; Kawashima, T.; Tomita, A.; Notomi, M.; Tamamura, T.; Sato, T.; Kawakami, S. *Phys. Rev. B* **1998**, *58*, 10096.
(5) Joannopoulos, J. D.; Villeneuve, P. R.; Fan, S. *Nature* **1997**, *386*, 143.
(6) Ogawa, S.; Imada, M.; Yoshimoto, S.; Okano, M.; Noda, S. *Science* **2004**, *305*, 227.
(7) Xia, Y. N.; Gates, B.; Yin, Y. D.; Lu, Y. *Advanced Materials* **2000**, *12*, 693.
(8) Ho, K. M.; Chan, C. T.; Soukoulis, C. M.; Biswas, R. M.; Sigalas, M. *Sol. Stat. Comm.* **1994**, *89*, 413.
(9) Busch, K.; John, S. *Phys. Rev. E* **1998**, *58*, 3896.
(10) Moroz, A. *Europhys. Lett.* **2000**, *50*, 466.
(11) Lopez, C. *Adv. Mater.* **2003**, *15*, 1679.
(12) Hynninen, A.-P.; Thijssen, J. H. J.; Vermolen, E. C. M.; Dijkstra, M.; Blaaderen, A. v. *Nat. Mater.* **2007**, *6*, 202.
(13) Joannopoulos, J. D.; Johnson, S. G.; Winn, J. N.; Meade, R. D. *Photonic Crystals: Molding the Flow of Light (Second Edition)*; Princeton University Press, 2008.
(14) Tarhan, II; Watson, G. H. *Physical Review Letters* **1996**, *76*, 315.
(15) Gourley, P. L.; Wendt, J. R.; Vawter, G. A.; Brennan, T. M.; Hammons, B. E. *Applied Physics Letters* **1994**, *64*, 687.
(16) Miguez, H.; Lopez, C.; Meseguer, F.; Blanco, A.; Vazquez, L.; Mayoral, R.; Ocana, M.; Fornes, V.; Mifsud, A. *Applied Physics Letters* **1997**, *71*, 1148.
(17) Garcia-Santamaria, F.; Lopez, C.; Meseguer, F.; Lopez-Tejeira, F.; Sanchez-Dehesa, J.; Miyazaki, H. T. *Applied Physics Letters* **2001**, *79*, 2309.
(18) Sözüer, H. S.; Haus, J. W.; Inguva, R. *Phys. Rev. B* **1993**, *45*, 13962.
(19) Vlasov, Y. A.; Bo, X.-Z.; Sturm, J. C.; Norris, D. J. *Nature* **2001**, *414*, 289.
(20) García-Santamaría; Ibisate, M.; Rodríguez, I.; Meseguer, F.; López, C. *Adv. Mater.* **2003**, *15*, 788.
(21) Li, Y.-J.; Xie, K.; Xu, J.; Du, P.-P. *Applied Physics a-Materials Science & Processing* **2010**, *99*, 117.
(22) Blanco, A.; Chomski, E.; Grabtchak, S.; Ibisate, M.; John, S.; Leonard, S. W.; Lo´pez, C.; Meseguer, F.; Mı´guez, H.; Mondia, J. P.; Ozin, G. A.; Toader, O.; Driel, H. M. v. *Nature* **2000**, *405*, 437.
(23) Noda, S.; Tomoda, K.; Yamamoto, N.; Chutinan, A. *Science* **2000**, *289*, 604.
(24) Palacios-Lidón, E.; Blanco, A.; Ibisate, M.; Meseguer, F.; López, C.; Sánchez-Dehesa, J. *Appl. Phys. Lett.* **2002**, *81*, 4925.
(25) Tetreault, N.; Miguez, H.; Ozin, G. A. *Advanced Materials* **2004**, *16*, 1471.
(26) Noda, S. *Mrs Bulletin* **2009**, *34*, 751.
(27) Rinne, S. A.; Garcia-Santamaria, F.; Braun, P. V. *Nature Photonics* **2008**, *2*, 52.
(28) Kress, A.; Hofbauer, F.; Reinelt, N.; Kaniber, M.; Krenner, H. J.; Meyer, R.; Bohm, G.; Finley, J. J. *Physical Review B* **2005**, *71*.
(29) Lodahl, P.; van Driel, A. F.; Nikolaev, I. S.; Irman, A.; Overgaag, K.; Vanmaekelbergh, D.; Vos, W. L. *Nature* **2004**, *430*, 654.
(30) Romanov, S. G.; Fokin, A. V.; De La Rue, R. M. *Applied Physics Letters* **1999**, *74*, 1821.
(31) Suezaki, T.; Yano, H.; Hatayama, T.; Ozin, G. A.; Fuyuki, T. *Applied Physics Letters* **2011**, *98*.
(32) Euser, T. G.; Wei, H.; Kalkman, J.; Jun, Y.; Polman, A.; Norris, D. J.; Vos, W. L. *Journal of Applied Physics* **2007**, *102*.
(33) Galisteo-Lopez, J. F.; Ibisate, M.; Sapienza, R.; Froufe-Perez, L. S.; Blanco, A.; Lopez, C. *Advanced Materials* **2011**, *23*, 30.
(34) Suezaki, T.; O'Brien, P. G.; Chen, J. I. L.; Loso, E.; Kherani, N. P.; Ozin, G. A. *Advanced Materials* **2009**, *21*, 559.
(35) Jiang, P.; Bertone, J. F.; Hwang, K. S.; Colvin, V. L. *Chemistry of Materials* **1999**, *11*, 2132.
(36) Johnson, P. M.; Koenderink, A. F.; Vos, W. L. *Physical Review B* **2002**, *66*.
(37) Lopez-Garcia, M.; Galisteo-Lopez, J. F.; Blanco, A.; Sanchez-Marcos, J.; Lopez, C.; Garcia-Martin, A. *Small* **2010**, *6*, 1757.
(38) Arpin, K. A.; Mihi, A.; Johnson, H. T.; Baca, A. J.; Rogers, J. A.; Lewis, J. A.; Braun, P. V. *Adv. Mater.* **2010**, *22*, 1084.
(39) Ning, H.; Mihi, A.; III, J. B. G.; Miyake, M.; Braun, P. V. *Adv. Mater.* **2012**, *24*, OP153.
(40) Sun, C.-H.; Jiang, P. *Nature Photonics* **2008**, *2*, 9.
(41) Gallego-Gomez, F.; Ibisate, M.; Golmayo, D.; Palomares, F. J.; Herrera, M.; Hernandez, J.; Molina, S. I.; Blanco, A.; Lopez, C. *Advanced Materials* **2011**, *23*, 5219.
(42) vanBlaaderen, A.; Ruel, R.; Wiltzius, P. *Nature* **1997**, *385*, 321.
(43) Velev, O. D.; Jede, T. A.; Lobo, R. F.; Lenhoff, A. M. *Nature* **1997**, *389*, 447.
(44) Zhou, Z. C.; Zhao, X. S. *Langmuir* **2005**, *21*, 4717.
(45) Hatton, B.; Mishchenko, L.; Davis, S.; Sandhage, K. H.; Aizenberg, J. *PNAS* **2010**, *23*, 10354.
(46) Sibu, C. P.; Kumar, S. R.; Mukundan, P.; Warrier, K. G. K. *Chemistry of Materials* **2002**, *14*, 2876.
(47) Brinker, C. J.; Scherer, G. W. **1990**.
(48) Shiohara, A.; Hanada, S.; Prabakar, S.; Fujioka, K.; Lim, T. H.; Yamamoto, K.; Northcote, P. T.; R. D. Tilley *J. Am. Chem. Soc.* **2010**, *132*, 248.
(49) Numata, M.; Koide, Y. *Beilstein Journal of Nanotechnology* **2010**, *1*, 71.
(50) Miclea, P. T.; Susha, A. S.; Liang, Z.; Caruso, F.; Torres, C. M. S.; Romanov, S. G. *Appl. Phys. Lett.* **2004**, *84*, 3960.
(51) Padmanabhan, S. C.; McGrath, J.; Bardosova, M.; Pemble, M. E. *J. Mater. Chem.* **2012**, *22*, 11978.
(52) Driel, H. M. v.; Vos, W. L. *Phys. Rev. B* **2000**, *62*, 9872.
(53) Nair, R. V.; Vijaya, R. *Phys. Rev. A* **2007**, *76*, 053805.
(54) Blanco, A.; López, C. *Adv. Mater.* **2006**, *18*, 1593.
(55) Tétreault, N.; Míguez, H.; Kitaev, V.; Yang, S. M.; Ozin, G. A. *Adv. Mater.* **2003**, *15*, 1167.
(56) Blanco, A.; Chomski, E.; Grabtchak, S.; Ibisate, M.; John, S.; Leonard, S. W.; Lopez, C.; Meseguer, F.; Miguez, H.; Mondia, J. P.; Ozin, G. A.; Toader, O.; van Driel, H. M. *Nature* **2000**, *405*, 437.
(57) Wang, D. Y.; Li, J. S.; Chan, C. T.; Sagueirino-Maceira, V.; Liz-Marzan, L. M.; Romanov, S.; Caruso, F. *Small* **2005**, *1*, 122.
(58) Lambropoulos, P.; Nikolopoulos, G. M.; Nielsen, T. R.; Bay, S. *Reports on Progress in Physics* **2000**, *63*, 455.
(59) John, S.; Quang, T. *Physical Review A* **1994**, *50*, 1764.
(60) Ogawa, S. P.; Imada, M.; Yoshimoto, S.; Okano, M.; Noda, S. *Science* **2004**, *305*, 227.
(61) Yamasaki, T.; Tsutsui, T. *Applied Physics Letters* **1998**, *72*, 1957.
(62) Petrov, E. P.; Bogomolov, V. N.; Kalosha, II; Gaponenko, S. V. *Physical Review Letters* **1998**, *81*, 77.
(63) Romanov, S. G.; Fokin, A. V.; Alperovich, V. I.; Johnson, N. P.; De La Rue, R. M. *Physica Status Solidi a-Applied Research* **1997**, *164*, 169.
(64) Vlasov, Y. A.; Deutsch, M.; Norris, D. J. *Applied Physics Letters* **2000**, *76*, 1627.
(65) Valenta, J.; Linnros, J.; Juhasz, R.; Rehspringer, J. L.; Huber, F.; Hirlimann, C.; Cheylan, S.; Elliman, R. G. *Journal of Applied Physics* **2003**, *93*, 4471.
(66) Warner, J. H.; Hoshino, A.; Yamamoto, K.; Tilley, R. D. *Angew. Chem. Int. Ed.* **2005**, *44*, 4550.
(67) Ledoux, G.; Guillois, O.; Porterat, D.; Reynaud, C.; Huisken, F.; Kohn, B.; Paillard, V. *Phys. Rev. B* **2000**, *62*, 15942.
(68) Boer, W. D. A. M. d.; Timmerman, D.; Dohnalova, K.; Yassievich, I. N.; Zhang, H.; Buma, W. J.; Gregorkiewicz, T. *Nat. Nanotechnol.* **2010**, *5*, 878.
(69) Wolkin, M. V.; Jorne, J.; Fauchet, P.; Allan, G.; Delerue, C. *Phys. Rev. Lett.* **1999**, *82*, 197.
(70) Gallego-Gómez, F.; Ibisate, M.; Golmayo, D.; Palomares, F. J.; Herrera, M.; Hernández, J.; Molina, S. I.; Blanco, Á.; López, C. *Adv. Mater.* **2011**, *23*, 5219.

(71) Sailor, M. J.; Wu, E. C. *Adv. Funct. Mater.* **2009**, *19*, 3195.
(72) Godefroo, S.; Hayne, M.; Jivanescu, M.; Stesmans, A.; Zacharias, M.; Lebedev, O. I.; Tendeloo, G. v.; Moshchalkov, V. V. *Nat. Nanotechnol.* **2008**, *3*, 174.
(73) Ma, J.; Parajuli, B. R.; Ghossoub, M. G.; Mihi, A.; Sadhu, J.; Braun, P. V.; Sinha, S. *Nano Letters* **2013**, *13*, 618.
(74) Birner, A.; Wehrspohn, R. B.; Gösele, U. M.; Busch, K. *13* **2001**, *6*, 377.
(75) Ibisate, M.; Golmayo, D.; Lpez, C. *Adv. Mater.* **2009**, *21*, 2899.
(76) Míguez, H.; Meseguer, F.; López, C.; Holgado, M.; Andreassen, G.; Mifsud, A.; Fornés., V. *Langmuir* **2000**, *16*, 4405.
(77) Míguez, H.; Chomski, E.; García-Santamaría, F.; Ibisate, M.; John, S.; López, C.; Meseguer, F.; Mondia, J. P.; Ozin, G. A.; Toader, O.; Driel, H. M. v. *Adv. Mater.* **2001**, *13*, 1634.
(78) Shimmin, R. G.; Vajtai, R.; Siegel, R. W.; Braun, P. V. *Chem. Mater.* **2007**, *19*, 2112.
(79) Seino, M.; Henderson, E. J.; Puzzo, D. P.; Kadotaa, N.; Ozin, G. A. *J. Mater. Chem.* **2011**, *21*, 15895.
(80) Norris, D. J.; Vlasov, Y. A. *Adv. Mater.* **2001**, *13*, 371.
(81) Yan, H.; Blanford, C. F.; Holland, B. T.; Parent, M.; Smyrl, W. H.; Stein, A. *Adv. Mater.* **1999**, *11*, 1003.
(82) Kulinowski, K. M.; Jiang, P.; Vaswani, H.; Colvin, V. L. *Adv. Mater.* **2000**, *12*, 833.
(83) Wijnhoven, J. E. G. J.; Zevenhuizen, S. J. M.; Hendriks, M. A.; Vanmaekelbergh, D.; Kelly, J. J.; Vos, W. L. *Adv. Mater.* **2000**, *2*, 888.
(84) Bartlett, P. N.; Baumberg, J. J.; Birkin, P. R.; Ghanem, M. A.; Netti, M. C. *Chem. Mater.* **2002**, *14*, 2199.
(85) Fu, M.; Zhou, J.; Xiao, Q.; Li, B.; Zong, R.; Chen, W.; Zhang, J. *Adv. Mater.* **2006**, *18*, 1001.
(86) Kassim, S.; Padmanabhan, S. C.; Salaun, M.; Pemble, M. E. *AIP Conf. Proc.* **2011**, *1391*, 263.
(87) Rugge, A.; Becker, J.; Gordon, R. G.; Tolbert, S. H. *Nano Letters* **2003**, *3*, 1293.
(88) King, J. S.; Graugnard, E.; Summers, C. J. *Adv. Mater.* **2005**, *17*, 1010.
(89) Povey, I. M.; Whitehead, D.; Thomas, K.; Pemble, M. E.; Bardosova, M.; Renard, J. *Appl. Phys. Lett.* **2006**, *89*, 104103.
(90) Graugnard, E.; Chawla, V.; Lorang, D.; Summers, C. J. *Appl. Phys. Lett.* **2006**, *89*, 211102.
(91) Trujillo, N. J.; Baxamusa, S. H.; Gleason, K. K. *Chemistry of Materials* **2009**, *21*, 742.
(92) Gaillot, D. P.; Summers, C. J. *Journal of Applied Physics* **2006**, *100*.
(93) One can tune the size of ncSis ss they are prepared prior to deposition process.

